

Robust Filtering of Artifacts in Difference Imaging for Rapid Transients Detection

J. Klencki, Ł. Wyrzykowski, Z. Kostrzewa–
Rutkowska and A. Udalski

Warsaw University Observatory, Al. Ujazdowskie 4, 00-478 Warszawa, POLAND
e-mail: jklencki@astrouw.edu.pl

ABSTRACT

Real-time analysis and classification of observational data collected within synoptic sky surveys is a huge challenge due to constant growth of data volumes. Machine learning techniques are often applied in order to perform this task automatically. The current bottleneck of transients detection in most surveys is the process of filtering numerous artifacts from candidate detection. We present a new method for automated artifact filtering based on hierarchical unsupervised classifier employing Self-Organizing Maps (SOMs). The system accepts 97% of real transients and removes 97.5% of artifacts when tested on the OGLE-IV Transient Detection System. The improvement of the artifacts filtering allowed for single-frame based rapid detections of transients within OGLE-IV, which now alerts on transient discoveries in less than 15 minutes from the image acquisition.

Key words:

1. Introduction

Over the last years, with large-scale sky surveys in their prime, the detection of rare supernovae-like transient events has been, to a large extent, successfully solved. Projects such as the Palomar Transient Factory (PTF, Law *et al.* 2009), the Catalina Real-Time Transient Survey (CRTS, Drake *et al.* 2009), PanSTARRS (Kaiser *et al.* 2010), the All-Sky Automated Survey for SuperNovae (ASAS-SN, *e.g.*, Shappee *et al.* 2014), the Optical Gravitational Lensing Experiment (OGLE, Wyrzykowski *et al.* 2014a, Udalski *et al.* 2015), Gaia Science Alerts program (Wyrzykowski *et al.* 2014b) and others are reporting numerous transient discoveries on a daily basis.

The remaining challenge, however, is to bring the transient detection process as close to real-time as possible. The quicker we discover an ongoing transient event, the sooner we are able to publish an alert, prompting extra follow-up observations. Early discovery of an ongoing event can also allow obtaining valuable spectroscopic observations (*e.g.*, PESSTO survey, Smartt *et al.* 2015). Ultimately, thanks to the follow-up started early, one can obtain far better data coverage than

that one would achieve when identifying the event only at, or after, its maximum brightness, which is, in turn, leading to better scientific results. For example, in the planetary microlensing detection, it is crucial to detect and intensively observe a very short-lived deviation from the standard model caused by a low-mass companion to the lens (*e.g.*, Udalski *et al.* 2005, Beaulieu *et al.* 2006, Skowron *et al.* 2015) in order to properly characterize the properties of the planet.

When working with supernovae (SNe) – which are usually the key focus of most transient surveys thanks to their cosmological applications (*e.g.*, Sullivan *et al.* 2011, Campbell *et al.* 2013 using SN Ia as "standardizable" candles following Phillips 1993) – good quality photometric and spectroscopic observations are essential for accurate standardization of SNe events, as well as for better understanding of the relations between characteristic properties of each event (*i.e.*, supernova's itself, its environment, etc.) and observed features in its light curve and spectra (*e.g.*, Childress *et al.* 2013a, 2013b, Galbany *et al.* 2014). Although thousands of supernovae events have been found up to date, only a small part of them have good enough data coverage from the very early days since explosion, sufficient to be studied effectively.

Other motivation for real-time supernovae detection is that we lack data points from the earliest stages of the events and these are the observations that carry information about the actual physics of supernovae explosion (*e.g.*, early-time spectrum revealing W-R-like wind signatures, Gal-Yam *et al.* 2014). Being able to obtain good quality photometry from before the maximum of brightness would allow for better verification of theoretical models of the most common SNe types, as well as possibly help understand the physics behind rarely observed exotic phenomena, such as, for example, super-luminous supernovae (*e.g.*, Quimby *et al.* 2011, Nicholl *et al.* 2015a, 2015b)

While the time scale of 'real-time' naturally depends on the type of transients we are looking for – varying from seconds in Gamma-Ray Bursts regime to days for long microlensing events caused by black holes – the constantly growing huge volumes of data are common for all kinds of sky surveys. With even bigger observational projects planned for the future (*e.g.*, LSST, Ivezić *et al.* 2008), it is clear that automation of data processing and analysis is inevitable. Current surveys' pipelines are already equipped with algorithms to perform observations, data reductions and calibrations automatically. Also the search for any changes in the brightness of observed objects, often carried out by time-domain surveys based on differential imaging technique, is done by the computers, resulting in numerous candidates for transient events. The remaining challenge of today's pipelines is to automatically perform the next stage, which is the actual filtering and classification of the vast volumes of the observational data.

Given the view of real-time transient detection, the advantages of computational (rather than human-based) technique are quite substantial:

- properly trained algorithms are much faster than human astronomer(s) ana-

lyzing individual data case by case. This allows triggering almost instantaneous follow-up observations and more effective usage of limited resources (observational time at telescope facilities) in order to obtain better data coverage;

- computational classification is deterministic, which also allows calibration of uncertainty. It appears that even experienced astronomers can have various opinions concerning same detection, which makes standardization uneasy (see Bloom & Richards, 2011)

The task of the automation itself, however, is not straightforward. The most promising approach is to implement machine-learning techniques. Many papers have been published recently on the subject, presenting automatic classification systems involved in different sky surveys. Wright *et al.* (2015) apply various machine-learning techniques for transient discovery in Pan-STARRS1 difference imaging, while Goldstein *et al.* (2015) searches for transients in the Dark Energy Survey. Eyer & Blake (2005) train the unsupervised Bayesian classifier of variable stars from the ASAS survey. Sánchez *et al.* (2010) employ k -means clustering to classify galactic spectra from the SDSS survey. Dubath *et al.* (2011) show how Random Forests can be applied in classification of variable stars from the Hipparcos mission. Bloom *et al.* (2012), by also implementing the Random Forest algorithm, develop the automated system for data analysis and preliminary classification in the PTF survey. Blagorodnova *et al.* (2014) take a Bayesian approach to classify transient events discovered by the Gaia satellite based on their low-resolution spectra. An excellent overview of the data mining and machine learning techniques in time-domain astronomy is presented by Bloom & Richards (2011). A more brief discussion of real-time transient search specifically can be found in Mahabal *et al.* (2012).

A specific type of classification problems is artifacts filtering. Finding candidates for transient events is very often overwhelmed by a huge number of unwanted artifacts, caused by cosmic rays, satellites' crossings, problems in reduction of images, misalignments of the images, CCD defects and others. Dealing with artifacts is extremely time-consuming as most of the work has to be done manually. Thus, the stage of selecting valuable candidates for transients is the current bottleneck of any transient survey and performing it automatically is an essential step towards real-time detections. In this paper we present a new method for robust, automatic artifact filtering and a transients detection system based on a hierarchical classifier of Self-Organizing Maps (SOMs). The most obvious advantage of SOMs is that they do not require preparation of any pre-classified and labeled training set which helps avoid potential biases introduced via the training set in supervised methods. The method has been applied to improve the detection purity and speed in the Optical Gravitational Lensing Experiment (OGLE) survey for transients (Wyrzykowski *et al.* 2014a) in its new, rapid generation.

The paper is organized as follows. In Section 2 we describe how the transients are searched in the OGLE-IV survey, where the data we use here come from. Section 3 shows how the artifact classifier is constructed. Section 4 describes the application of the new classifier to the new rapid transient search in OGLE-IV. We conclude in Section 5.

2. Transients Detection in OGLE-IV

The Optical Gravitational Lensing Experiment has been started in 1992 (first phase: OGLE-I) as one of the first surveys dedicated to gravitational microlensing events. The current phase of the project (OGLE-IV, since 2010) is conducted on a 1.3 meter Warsaw Telescope located at the Las Campanas Observatory, Chile, operated by the Carnegie Institution for Science. The telescope is equipped with a large field CCD mosaic camera with 32 CCD detectors ($2x \times 4k$ each) – one of the largest CCD mosaics worldwide. It covers the entire field of view of the Warsaw telescope (1.4 square degrees; scale $0.''26$ /pixel). The OGLE-IV project carries out observations in two filters of Johnson/Cousins photometry system: the *I*- and *V*-band, with the majority of observations being done using the former. More technical details of the survey can be found in Udalski *et al.* (2015).

OGLE-IV observations cover the Galactic bulge, disk and the Magellanic Clouds and their surroundings. The extragalactic transients are being search for in the region covering about 650 square degrees toward the Magellanic Clouds System (MCS). Some of those regions have been regularly observed since 2010, which resulted in a huge database of objects with variability monitored over years. The typical cadence of MCS observations is from two to five days, depending on the time in the season (typically from August until April), resulting in few hundreds of frames collected per field.

The area around Magellanic Clouds is observed primarily in the *I*-band and with exposure of 150 seconds. Read-out time for 32-CCD-chip mosaic is about 20 seconds (Udalski et al. 2015). In the next minute after data acquisition the reduced (bias-subtracted and flat-fielded) image is ready for further processing.

Since the primary motivation for creating the OGLE project was the search for microlensing events, which occur in the most dense stellar regions, the OGLE have mastered the difference imaging technique to achieve the best results in those challenging sky regions. The Difference Imaging Analysis (DIA) method tuned to the OGLE data is based on the Woźniak (2000) implementation of Alard & Lupton (1998) algorithm. The reference images for the DIA method are obtained by stacking several high-quality images obtained under perfect seeing conditions (less than $1''$).

The data processing pipeline reduces incoming images on-the-fly and after about three minutes the subtracted image is produced along with detections of new sources, their positions and preliminary magnitudes. The match to Gaussian profile

of each brightening must exceed 0.7, with 1.0 interpreted as a perfect match, as we are looking for point sources. Subtractions fulfilling those conditions are accepted as candidates, cross-matched with OGLE’s database of known stellar-like objects and divided into two channels: *old sources* (*i.e.*, brightenings of previously known objects) and *new sources* (*i.e.*, brightenings appearing as new objects). Because most of the galaxies are not in the OGLE’s stellar-like objects database the investigation of candidates from the new source channel is ideal for the search for exo-galactic transients such as supernovae. Brightenings detection from the old source channel, on the other hand, are mostly caused by variable stars and cataclysmic variables.

The search for transients in years 2012–2014 (Wyrzykowski *et al.* 2014a) required two subsequent detections of a candidate transient to ensure high purity of discoveries. The selected candidates (typically 100–300 each night) were visually inspected and promising transients were picked based on contextual information (*e.g.*, galaxy nearby) and archival data (previous variability or non-detections).

3. Artifact Filtering Classifier

As can be expected, the vast majority of transient candidates from data reduction pipeline are unwanted artifacts. The most common are four types of artifacts: (a) satellites’ crossings, (b) cosmic rays, (c) image subtraction defects and (d) ”yin-yang” shapes caused by stellar objects with high proper motion. Fig. 1 shows examples of artifacts as seen in the difference images produced by the OGLE pipeline. Avoiding the most common types of artifacts, types (a) and (b), can be easily achieved by the requirement for repeating observations of the same field. However, such method stands against the idea of bringing transient detection as close to real-time as possible, as in OGLE’s case the detectability time frame is then limited by our cadence of 2–5 days. This is a trade-off between the number of repeated observations versus the sky area covered. In order to allow for very rapid discovery of transients with the current OGLE observing strategy we aimed at filtering the artifacts based on a single OGLE observation.

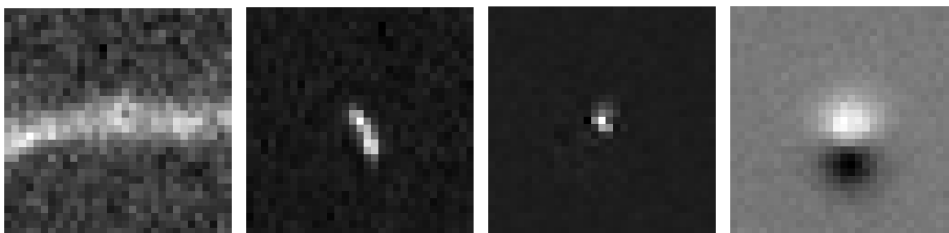


Fig. 1. Most common types of artifacts from the OGLE transient pipeline presented as 31×31 pixel cutouts from difference images. *Left panel* shows satellite’s crossing artifact and *two next panels* – cosmic ray and subtraction failure (too faint) artifacts. The *most right* panel presents high proper motion stellar object artifact.

3.1. The Tool: Self-Organizing Map

Self-Organizing Map (SOM, Kohonen 1982), is an example of an unsupervised artificial neural network, which has a huge potential in astronomical data analysis problems (see Wyrzykowski & Belokurov, 2008). The ability to organize itself helps when dealing with classes of objects with not well defined boundaries. The network is usually arranged into a two-dimensional array of nodes with *weight vectors* \mathbf{w} associated to them. Each analyzed datum, in our case a 31x31 pixel cutout image of brightening, is represented in form of a numeric vector \mathbf{t} (of same length as weight vectors) and mapped onto node with weight vector \mathbf{w}_0 most similar to it – the winner node. The usual criteria for similarity is the least Euclidian distance between vectors, *i.e.*, the following condition is fulfilled:

$$\forall \mathbf{w} \in \text{SOM} \quad |\mathbf{w} - \mathbf{t}| \geq |\mathbf{w}_0 - \mathbf{t}| \quad (1)$$

The SOM organizes itself during an unsupervised learning process. The initial values of weight vectors can be set according to some pattern, for instance linearly growing. However, for a sufficiently long training loop the initial conditions do not affect the final form of SOM in any noticeable way. Then, for each training vector \mathbf{t} (chosen either randomly or one by one from the training dataset) the winner node \mathbf{w}_0 is found. The actual learning process takes place now, when the winner \mathbf{w}_0 and all its neighboring nodes are adjusted with a learning rate $\alpha(\mathbf{n})$ in order to become more similar to the training vector \mathbf{t} . For the step number n of the training loop the learning process will be as follows:

$$\mathbf{w}_{\text{new}} = \mathbf{w}_{\text{old}} + \alpha(n)(\mathbf{t} - \mathbf{w}_{\text{old}}) \quad (2)$$

The learning rate $\alpha(\mathbf{n})$ decreases from 1 to 0 during the whole training process, typically in a linear way.

3.2. Data Representation

The key element of a SOM-based classifier is the way of representing each analyzed datum in form of a numeric vector. It should contain all the information needed for a successful classification and in the same time the vector should not be too long (longer vector means longer calculation time). In this case for each transient candidate we first produce a 31x31 pixel cutout from the difference image centered on the brightening. The image values are normalized in such a way, that the brightest pixel always has the value 1.0 and the mean background level corresponds to 0.5 – this means that we only analyze the profile (shape) of the brightening, without considering the absolute value of brightening at this stage. We also perform the *angle normalization* of cutouts, that is rotate each of them by an angle of 0° , 90° , 180° or 270° in such a way, that the brightest half-part of the image (*i.e.*, having biggest sum of pixel values) is always the top one. This way we reduce by half the number of somewhat artificial types of brightenings appearing

due to their random orientation. Normalized cutouts are then represented in form of numeric vectors of length 1061: the first $961 = 31^2$ fields are simply the values of the cutout's pixels and the last 100 fields correspond to heights of the bins of a normalized histogram of the image. This representation, similar to that adopted by Wright *et al.* (2015) for transient detection in the Pan-STARRS1 survey, differs from most of previous work in that it works directly on the pixel's values rather than on specific features of the image.

3.3. Hierarchical Classifier

We trained a triple-stage SOM classifier for transients detection from OGLE. The first stage (*Anti-cosmic SOM*) is responsible for ruling out the majority of the artifacts of most numerous types: satellites' crossings and cosmic rays. At the second stage (*Anti-yinyang SOM*) the classifier eliminates most of the "yin-yang"-like objects and the remaining cosmic rays. The final stage map (*Anti-faint SOM*) is aimed at dealing with those types of artifacts that the second stage SOM failed to exclude – which are mostly image subtraction defects appearing as brightening too faint to be caused by a real transient event. Each stage's SOM has a form of an independent two-dimensional array of five nodes width and seven nodes height.

The first stage: Anti-Cosmic SOM

We prepared a set of input data based on difference imaging produced by the OGLE data reduction pipeline. All new objects (not matched to known reference objects) brighter than about 19.5 mag were gathered from the period of a couple of months in early 2014. The training data set comprised of 7000 detections found based on a single frame observation, hence consisting primarily of cosmic rays and satellites' crossings. The training loop had 50 000 steps with learning parameter set as a constant value $\alpha = 0.2$. The radius of nodes treated as neighbors was set to three. The trained map is presented in Fig. 2a.

When using SOM as an artifact filtering tool one has to choose which nodes form the *acceptance region* of the verification system, *i.e.*, transient candidates classified into those nodes are verified as positive and accepted, whereas the rest is treated as artifacts and ruled out. In order to determine the best possible acceptance region we decided, as a rule, to prioritize nodes with highest "purity" P (Bloom *et al.* 2012) defined as:

$$P = \frac{R_{acc}(real)}{R_{acc}(real) + R_{acc}(artifact)} , \quad (3)$$

The rate of accepting certain "type" as "real" or "artifact" – can be expressed as:

$$R_{acc}(type) = R(type) \cdot P(acceptance | type) , \quad (4)$$

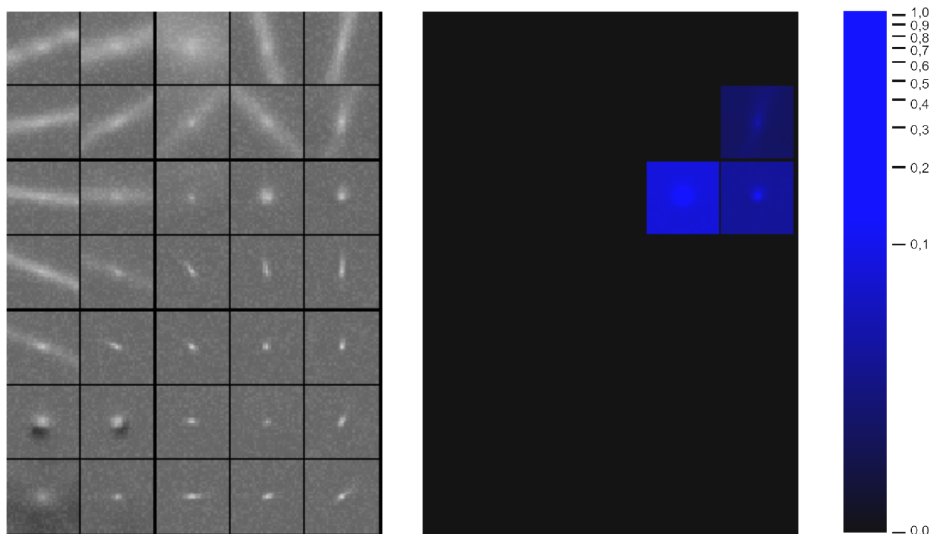


Fig. 2. Anti-cosmic SOM – map trained for the first stage of artifacts filtering classifier. *Left panel* shows visualization of the nodes of the trained SOM. *Right panel* presents map of relative purity of nodes based on the test set.

which is the rate of occurrence of the type in the analyzed data population $R(\text{type})$ multiplied by the probability of it being accepted by the node.

In order to calculate the purity of each node we performed a test classification on a dataset of more than 13 200 images, which contained 89 images of known good transients (chosen manually from transients selected during the OGLE Transient Search). The probabilities $P(\text{acceptance} | \text{type})$ for each node were estimated as:

$$P(\text{acceptance} | \text{type}) = \frac{\# \text{ accepted candidates of the type}}{\# \text{ all candidates of the type in the dataset}} \quad (5)$$

Based on the test classification we obtained a map of relative nodes' purity, normalized to range [0,1] (see Fig. 2b). The map clearly shows that known real transients landed in only three nodes (purity larger than 0). Those three nodes accepted altogether all 89 real transient detections and 599 of nearly 13 200 artifacts, which corresponds to the false positive ratio (FPR) of $FPR_{I \text{ stage}} \approx 0.045$ and the true positive ratio (TPR) being $TPR_{I \text{ stage}} = 1.0$. Naturally, these nodes formed the acceptance region for the first stage of the classifier.

The Second Stage: Anti-Yinyang SOM

The second stage SOM has been trained on a different training dataset than in the first stage. It contained about 12 000 images of detections from the OGLE pipeline which were selected requiring at least two independent observations at the same location on two subsequent frames, again with 19.5 mag threshold for both of the detections. The brighter of the two was chosen for the training set. Thanks to

that selection most of the artifacts caused by cosmic rays and satellites' crossings were not present in that dataset. The training loop had 100 000 steps with learning parameter set as a constant value $\alpha = 0.2$. The radius of nodes treated as neighbors was set to three. The trained map is presented in Fig. 3a.

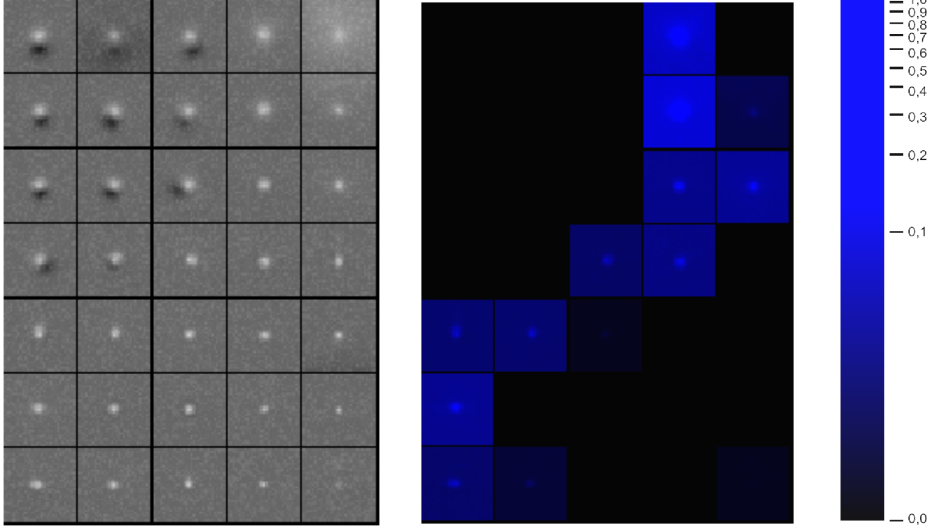


Fig. 3. Anti-yinyang SOM – map trained for the second stage of artifacts filtering classifier. *Left panel* shows visualization of the nodes of the trained SOM. *Right panel* presents map of relative purity of nodes based on the test set.

The acceptance region was determined based on a test classification of over 12 400 detections, requiring their presence on the same location in at least two subsequent frames. It contained transient events detected and confirmed by long term monitoring by the OGLE in years 2012–2014 (total of 327 real transients). Based on the classification we obtained a map of normalized relative nodes' purity, following the procedure described above – see Fig. 3b. At this stage there were multiple nodes with positive purity. We included all of them to the acceptance region, resulting with all 327 real transient detection as well as 6859 artifacts being accepted, which corresponded to the false positive ratio of $FPR_{II\ stage} \approx 0.57$ and true positive ratio of $TPR_{II\ stage} = 1.0$. It shows that it is much more difficult to obtain pure classifier performance at the second stage in comparison to the first stage ($FPR_{I\ stage} \approx 0.045$ and $TPR_{I\ stage} = 1.0$), as the most obvious and easy to recognize artifacts were already filtered out at the first stage.

The Third Stage: Anti-Faint SOM

To improve the performance of the non-cosmic artifacts elimination from the second stage we trained the third, final stage SOM aimed at recognizing those types of defects the second stage SOM failed to distinguish from real transient detections. The training set was thus composed of the 7186 candidates that were accepted at

the second stage's test classification: 327 confirmed transients and 6859 artifacts. The training loop had 100 000 steps with learning parameter set as a constant value $\alpha = 0.2$. The radius of nodes treated as neighbors was set to three. The trained map is presented in Fig. 4a.

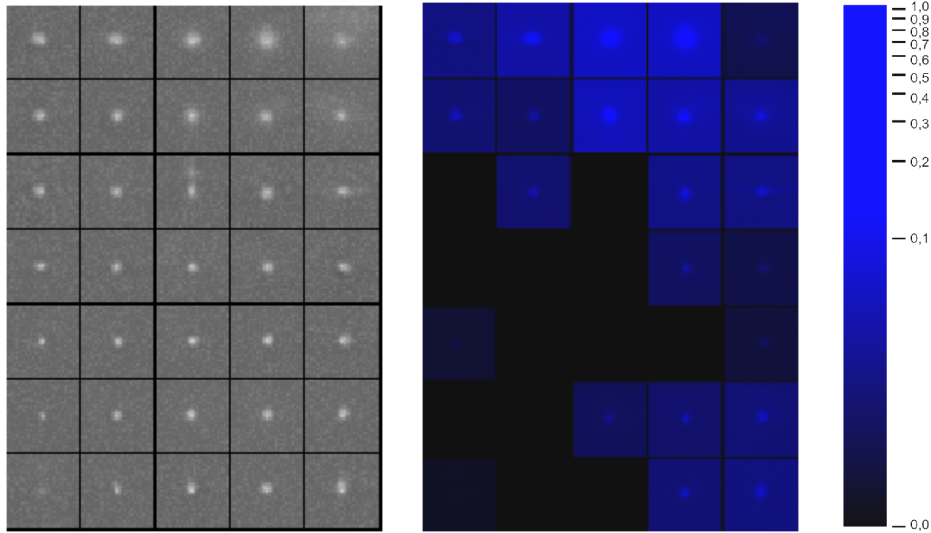


Fig. 4. Anti-faint SOM – map trained for the third stage of artifacts filtering classifier. The training dataset consisted of 7186 images of OGLE detections that were passed by the second stage SOM. *Left panel* shows visualization of the nodes of the trained SOM. *Right panel* presents map of relative purity of nodes based on the test set.

The acceptance region was determined based on a test classification of same database of 7186 candidates. A map of normalized relative nodes' purity was drawn following the procedure described in Section 3.4 – see Fig. 4b. At the final stage the choice of acceptance region is more difficult than at previous stages as most of the nodes express positive purity. The more nodes we included into the acceptance region, the lower the false negative ratio ($FNR = 1 - TPR$), however, the false positive ratio increases alongside – something we would very much like to avoid. This fact is illustrated by the receiver operating characteristic (ROC) curve, which plots FPR with respect to FNR for different sizes of the acceptance region (see Fig. 5).

3.4. Triple-Stage Classifier's Performance

In order to decide on the number of nodes forming the acceptance region at the third stage we investigated the behavior of the fully operating, triple-stage classifier. We performed test classification of over 13 000 candidate detections from the OGLE pipeline gathered without the requirement of having at least two independent observations, *i.e.*, based solely on a single observation. The acceptance region at the first and second stage were set as discussed above. By varying the size of

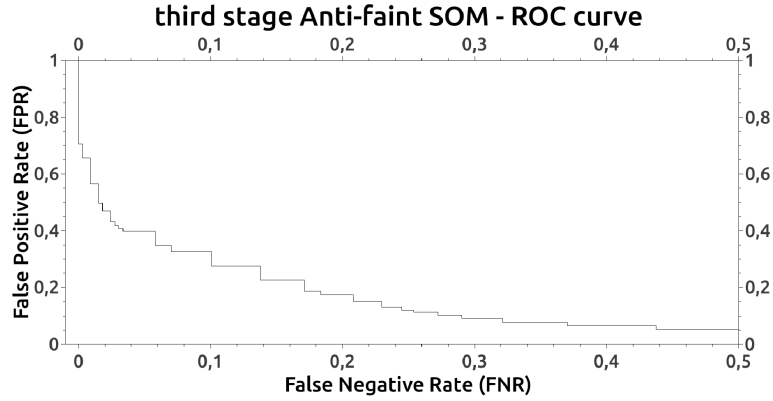


Fig. 5. Receiver operating characteristic (ROC) curve for the third-stage SOM.

the third stage acceptance region we obtained different FPR to FNR ratios for the entire triple-stage classifier, as presented in form of the ROC curve in Fig. 6.

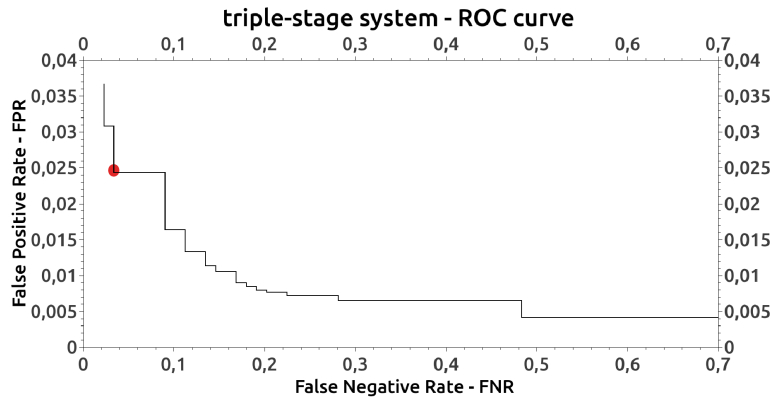


Fig. 6. Receiver operating characteristic (ROC) curve for the entire triple-stage artifact filtering classifier based on result of a test classification of 13 000 candidate detections from the OGLE pipeline, generated without the requirement of having at least two independent observations. For the chosen threshold (red dot) the system accepts $\approx 97\%$ of real transient detections and excludes $\approx 97.5\%$ of artifacts from the data.

For an exemplary and satisfactory threshold (marked on the ROC curve with a red dot) the system accepts $\approx 97\%$ of real transient detections and excludes $\approx 97.5\%$ of artifacts from the data. The purity of the candidates database (here the percentage of real transient detections) has increased to the final purity of $\approx 26\%$ from the initial value of 0.7% . This is a huge improvement, as the remaining number of daily candidates can be easily inspected and verified manually in close to real-time time-frame. It is worth noting that the classifier relied solely on the difference images and did not employ any light curve nor contextual information around the transient candidate.

4. Application: Rapid OGLE Transients Detection System

OGLE-IV has been running a search for transients objects, OGLE Transients Detection System (OTDS, Kozłowski *et al.* 2013, Wyrzykowski *et al.* 2014a) since 2012. This dedicated survey has discovered so far about 500 various transients, primarily supernovae and novae. The spectroscopic classification and follow-up has been provided primary thanks to collaboration with the PESSTO group (Smartt *et al.* 2015) for about 100 targets, which resulted in findings of rare and interesting transients (*e.g.*, Inserra *et al.* 2015, Poznanski *et al.* 2015, Pastorello *et al.* 2015).

The triple-stage SOM-based classifier has been applied in a new version of the OGLE Transient Detection System, the OTDS-Rapid. High efficiency of the artifact filtering allowed for a substantial increase in the speed of detection of new transients within the OGLE-IV pipeline. The original OTDS required two subsequent frames to contain a transient, in order to filter out numerous contaminants and false detections. This, however, resulted in belated discoveries of transients, given our sampling strategy. The new OTDS-rapid relies solely on a single frame exposure taken by the OGLE-IV survey and is able to produce transient discoveries within less than 15 minutes after data acquisition.

The ODTS-Rapid pipeline analyzes each of the new sources (not linked to any of the known old OGLE sources during the cross-match). At the magnitude threshold currently set at 19.5 mag there is from 10 to 50 new sources detected per chip, meaning 320 to 1600 sources to investigate with every frame. For a typical night, there is in total about 25 000 new sources to investigate. After the triple-stage SOM artifact classifier, there remains about a 100 of candidates. For those, the force-photometry is obtained: on known position of the potential transient we measure photometry on the current and 10 most recent previous frames. Only the objects for which there is at least six previous non-detections are carried over to the next stage. For transients located at galactic cores we rule out AGN-like object using WISE colors, applying the criteria of Assef *et al.* (2010). We also compute the offset from the nearest galaxy-like object, which were detected on the OGLE reference images (Kostrzewa-Rutkowska *et al.* in prep.). The accuracy of the offset computation is better than $0.''13$ (Wyrzykowski *et al.* 2014a). In a typical night there is about 10 to 30 candidates selected in a completely autonomous manner. The webpage:

<http://ogle.astrouw.edu.pl/ogle4/transients/rapid/rapid.html>

is updated every 5 minutes and contains the most recent discoveries carried out by the OTDS-Rapid, which are available for the astronomical community to select targets for further immediate follow-up. Fig. 7 shows an example discovery of OGLE15hy, which turned out to be a type Ia supernova. The time from the observation to the moment the object appeared on the webpage was about 15 minutes.

At a conservative threshold of $I = 19.5$ mag we are already able to detect supernovae type Ia at about 2 magnitudes before their maximum brightness for a typical

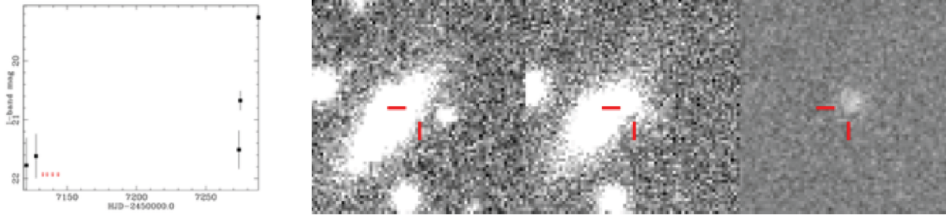


Fig. 7. Example rapid detection of OGLE15hy type Ia supernova in about 15 minutes after the observation. *Left panel* shows the light curve at the moment of the discovery with magnitude threshold at $I = 19.5$. Pre-discovery data points were obtained by force-photometry at the position of the transient. The red arrows indicate non-detections. *Right panel*: reference, current and difference image of the transient. Size $18'' \times 18''$.

redshift in our survey of $z = 0.07$. For a more ambitious threshold of $I = 20.5$ mag (number of artifacts increases to about 40 every night) we reach a capability of discovering supernovae type Ia at about -10 to -20 days prior to their maximum. Rapid detections help organize the follow-up observations early and investigate the earliest stages of supernova explosion, providing clues on supernova origin.

5. Conclusions

Modern large-scale sky surveys have become very successful in discovering rare transient events such as supernovae, thanks to collecting increasingly huge volumes of observational data. Thousands of candidates for transients are generated every day by repeatedly analyzing same fields in search for unexpected brightness changes. Manual verification of so many detections in a short time-frame from the observation begins to exceed capabilities of observers. Thus, real-time transient detection – the ultimate goal of transient surveys – still remains a big challenge. The main problem lies in extremely numerous artifact brightennings among transient candidates, easy to identify by a watchful eye of an experienced astronomer but difficult to deal with automatically. The usual way of eliminating the most common bogus detections (randomly appearing cosmic rays and satellites' crossing) is by requiring the subtraction residual to appear on at least two independent sky frames. This approach has a major drawback, however, as it limits the detectability-frame to the sampling of the survey and often significantly slows down the detection process.

In this work we presented a new method for robust artifact filtering based on a hierarchical machine-learning classifier composing of self-organizing maps (SOMs). The triple-stage system has been trained on transient candidates from the OGLE Transient Detection System in order to eliminate the most popular types of artifacts. The classifier performance has been optimized to a typical population of detections in the OGLE survey and tested on a representative dataset of transient candidates. For a chosen threshold the system accepts $\approx 97\%$ of real transient detections and excludes $\approx 97.5\%$ of artifacts from the data. This result is satisfactory

and sufficient for replacing the former requirement for two independent observations and gives birth to the new Rapid Transient Detection System in the OGLE project. The transient detections can now be carried out in less than 15 minutes from the observation, which is closer to real-time than it has ever been ever.

Acknowledgements. This work was supported by the Polish National Science Center grant no. 2015/17/B/ST9/03167 to ŁW. The OGLE project has received funding from the Polish National Science Centre grant MAESTRO no. 2014/14/A/ST9/00121 to AU.

REFERENCES

- Alard, C., Lupton, R. H. 1998, *ApJ*, **503**, 325.
Assef, R. J. *et al.* 2010, *ApJ*, **713**, 970.
Beaulieu, J. -P. *et al.* 2006, *Nature*, **439**, 437.
Blagorodnova, N. *et al.* 2014, *MNRAS*, **442**, 327.
Bloom, J., Richards, J. W. 2011, , , arXiv:1104.3142.
Bloom, J. *et al.* 2012, *PASP*, **124**, 1175.
Campbell, H. *et al.* 2013, *ApJ*, **763**, 88.
Childress, M. *et al.* 2013a, *ApJ*, **770**, 107.
Childress, M. *et al.* 2013b, *ApJ*, **770**, 108.
Drake, A. J. *et al.* 2009, *ApJ*, **696**, 870.
Dubath, P. *et al.* 2011, *MNRAS*, **414**, 2602.
Eyer, L., Blake, C. 2005, *MNRAS*, **358**, 30.
Gal-Yam, A. *et al.* 2014, *Nature*, **509**, 471.
Galbany, L. *et al.* 2014, *A&A*, **572**, A38.
Goldstein, D. A. *et al.* 2015, *AJ*, **150**, 82.
Inserra, C. *et al.* 2015, *ApJ*, **799**, L2.
Ivezić, Z. *et al.* 2008, , , arXiv:0805.2366.
Kaiser, N. *et al.* 2010, SPIE Conference Series, Vol. 7733.
Kohonen, T. 1982, *Biological Cybernetics*, **43**, 59.
Kozłowski, S. *et al.* 2013, *Acta Astron.*, **63**, 1.
Law, N. M. *et al.* 2009, *PASP*, **121**, 139.
Mahabal, A. A. *et al.* 2012, *IAU Symposium*, **285**, 355.
Nicholl, M. *et al.* 2015a, *ApJ*, **807**, L18.
Nicholl, M. *et al.* 2015b, *MNRAS*, **452**, 3869.
Pastorello, A. *et al.* 2015, *MNRAS*, **449**, 1941.
Phillips, M. M. 1993, *ApJL*, **413**, L105.
Poznański, D. *et al.* 2015, *MNRAS*, **449**, 1753.
Quimby, R. M. *et al.* 2011, *Nature*, **474**, 487.
Sánchez, A. J. *et al.* 2010, *ApJ*, **714**, 487.
Shappee, B. *et al.* 2014, *ApJ*, **788**, 48.
Smartt, S. J. *et al.* 2015, *A&A*, **579**, A40.
Skowron, J. *et al.* 2015, *ApJ*, **804**, 33.
Sullivan, H. *et al.* 2011, *ApJ*, **737**, 102.
Udalski, A. 2003, *Acta Astron.*, **53**, 291.
Udalski, A. *et al.* 2005, *ApJ*, **628**, L109.
Udalski, A., Szymański, M.K., and Szymański, G. 2015, *Acta Astron.*, **65**, 1.
Woźniak, P. R. *et al.* 2000, *Acta Astron.*, **50**, 421.
Wright, D. E. *et al.* 2015, *MNRAS*, **64**, 197.

Wyrzykowski, L., and Belokurov, V. 2008, *American Institute of Physics Conference Series*, **1082**, 201.

Wyrzykowski, L. *et al.* 2014a, *Acta Astron.*, **65**, 1.

Wyrzykowski, L., Hodgkin, S., Blagorodnova, N., and Belokurov, V. 2014b, *IAU Symposium*, **298**, 446.